Size-Selective Carbon Clusters as Obstacles to Graphene Growth on a Metal

Alexandre Artaud,[†,‡] Laurence Magaud,[‡] Kitti Ratter,[¶,‡] Bruno Gilles,[¶,‡] Valérie Guisset,[‡] Philippe David,[‡] Jose Ignacio Martinez,[§] Jose Angel Martin-Gago,[§] Claude Chapelier,[†] and Johann Coraux[*,‡]

†*Univ. Grenoble Alpes, CEA, INAC, PHELIQS, 38000 Grenoble, France*

‡*Univ. Grenoble Alpes, CNRS, Grenoble INP, Institut NEEL, 38000 Grenoble, France*

¶*Univ. Grenoble Alpes, CNRS, Grenoble INP, SIMAP, 38000 Grenoble, France*

§*Materials Science Factory, Instituto de Ciencia de Materiales de Madrid-CSIC, C/Sor Juana Inés de la Cruz 3, Madrid 28049, Spain*

E-mail: johann.coraux@neel.cnrs.fr

Abstract

Chemical vapor deposition (CVD) on metals is so far the best suited method to produce high quality large-area graphene. We discovered an unprecedentedly large family of small size-selective carbon clusters that form together with graphene during CVD. Using scanning tunneling microscopy (STM) and density functional theory (DFT), we unambiguously determine their atomic structure. For that purpose we use grids based on a graphene moiré and a dilute atomic lattice that unambiguously reveal the binding geometry of the clusters. We find that the observed clusters bind in metastable configurations on the substrate, while the thermodynamically stable configurations are not observed. We argue that the clusters are formed under kinetic control and establish that the evolution of the smallest clusters is blocked. They are hence products of surface

reactions in competition with graphene growth, rather than intermediary species to the formation of extended graphene, as often assumed in the literature. We expect such obstacles to the synthesis of perfect graphene to be ubiquitous on a variety of metallic surfaces.

Keywords

Carbon clusters, Metastability, Kinetics, Graphene, Graphene growth, Scanning tunneling microscopy, Density functional theory

Introduction

Graphene, as a monolayer of sp^2-hybridized carbon atoms, has emerged over the past few years not only as a prototypical two-dimensional material with remarkable electronic properties,[1] but also by raising interest for electronic, optoelectronic or biosensing applications.[2] The historical micromechanical cleavage method produces high-quality samples, but cannot be scaled up at the industrial level. In contrast, CVD provides an excellent compromise between yield and sample quality, making it an ideal method for large-scale applications. CVD consists in the exposure of a metallic surface to a hydrocarbon precursor at a high enough temperature, and relies on the metal's catalytic activity to decompose the precursor and promote the formation of graphene. Over the years, this method has been successfully developed on a large variety of transition metals, such as Cu, Ir, Pt, Ni, Ru, Rh, Re to name a few.[3]

Among the possible substrates, Ru(0001), Rh(111) and Re(0001) constitute a family of metals, whose d electronic bands lie close to the Fermi level and strongly hybridize with graphene's π bands, leading to short C-metal bonds.[4] Consequently, they favor a single orientation of graphene,[3] making them attractive candidates to grow large-scale single-domain graphene with high crystalline quality. This single orientation also gives rise to well-defined

moiré patterns, which have been used in turn as templates to deposit molecules[5] or size-selective metallic clusters,[6,7] in the pursuit of applications such as magnetic data storage or spintronics.[8] It is also worth noting Re(0001) has raised fundamental interest, as it is a platform where both spin-orbit coupling[9] and induced superconductivity[10] can coexist.

The strong affinity of this family of metals with carbon also results in the formation of phases competing with graphene growth. Indeed, surface carbide formation is promoted on Rh(111)[11] and Re(0001)[12,13] at high enough temperature. Moreover, at even higher temperatures, bulk dissolution of carbon is favored for Ru(0001),[14] Rh(111),[11] and Re(0001).[13] Graphene growth on Ru(0001) and Rh(111) is also very similar, as it proceeds through three temperature-programmed regimes. First, below ∼700 K, the hydrocarbon precursors decompose in several steps as the temperature is raised, until their full dehydrogenation at ∼700 K.[15] STM images and high resolution electron energy loss spectra acquired at different steps of graphene growth on Ru(0001) suggest a similar scenario.[16,17]

At higher temperature (typically $700 - 1000$ K) such that extended graphene forms, the carbon species reported on the surface are of two kinds : C monomers and various size-selective carbon clusters.[11,15–20] Finally, for temperatures higher than ∼1000 K, elementary carbon atoms are the only remaining species,[15,21] so graphene growth proceeds exclusively by attachment of C monomers and short C chains.[22]

The Ru(0001) and Rh(111) surfaces promote the formation of two specific size-selective C clusters (various small-size clusters were also observed on Pt(111)[23,24] and Ir(111),[25,26] but whether they are size-selective is unknown so far). These clusters were observed with STM. It was proposed that they are composed of three and seven hexagonal rings,[17,20] ~~(3C6 and 7C6),~~ which corresponds to the structure of dehydrogenated phenalene and coronene respectively, as illustrated on Figures 1*b,d*. However, later DFT studies put this claim into question on two grounds: first, the much higher stability of pentagon-membered molecules of similar size, and second, the better agreement obtained by simulating STM images with these molecules.[27–29] In particular, the seven-hexagon-cluster~~7C6~~ cluster identification is re-

interpreted as a more stable cluster, whose structure consists of a central hexagonal ring surrounded by alternating hexagonal and pentagonal carbon rings (C_{21}~~4C6-3C5~~), similar to a dehydrogenated sumanene molecule.[27] In fact, the difficulty in unambiguously determining the cluster is inherent to STM imaging, which a priori does not distinguish chemical and structural features. The way the clusters bind on the substrate is here crucial, since it sets the precise chemical nature of the individual atoms of the cluster. Information to this respect could not be determined in experimental reports so far.[11,15–20,25] Probably for this reason, a conclusive discussion on the stability of the C clusters was, to a large extent, left aside.

In the present work we have studied the formation of graphene on the Re(0001) surface. Atomically-resolved STM data compared to the result of DFT calculations reveal a strikingly diverse family of size-selective C clusters. By discriminating crystallographic sites of the metal surface that usually appear undiscerned in STM, we disclose how the clusters bind on the metal surface. For that purpose we introduce a tool, the chemical equivalent of magnifying lenses, in the form of atomic masks consisting of a moiré nanopattern between graphene and Re(0001), or of a dilute atomic lattice (here made of carbon). This way we manage to solve the puzzle of the identification of the C clusters, and find dehydrogenated polycyclic molecules, one made of three hexagonal rings (13 carbon atoms, C_{13}), another one made of three open hexagonal rings, one close hexagonal ring and three pentagonal rings (C_{21}), and three other, larger ones consisting exclusively of hexagonal rings.~~3C6, 7C6, 4C6-3C5, and two larger three-fold symmetric dehydrogenated polycyclic molecules (12C6 and 18C6).~~ We argue that the observed clusters are metastable and not the lowest-energy intermediates towards the growth of graphene, at variance to the common wisdom. The formation and the transformation of the observed clusters, and expectedly as well of those reported by others,[11,15–19] appears kinetically blocked rather than dictated by thermodynamics considerations. The smallest of these clusters even appears to be an obstacle towards the growth of perfect graphene, and coexists with the latter up to advanced stages of preparation.

Results and Discussion

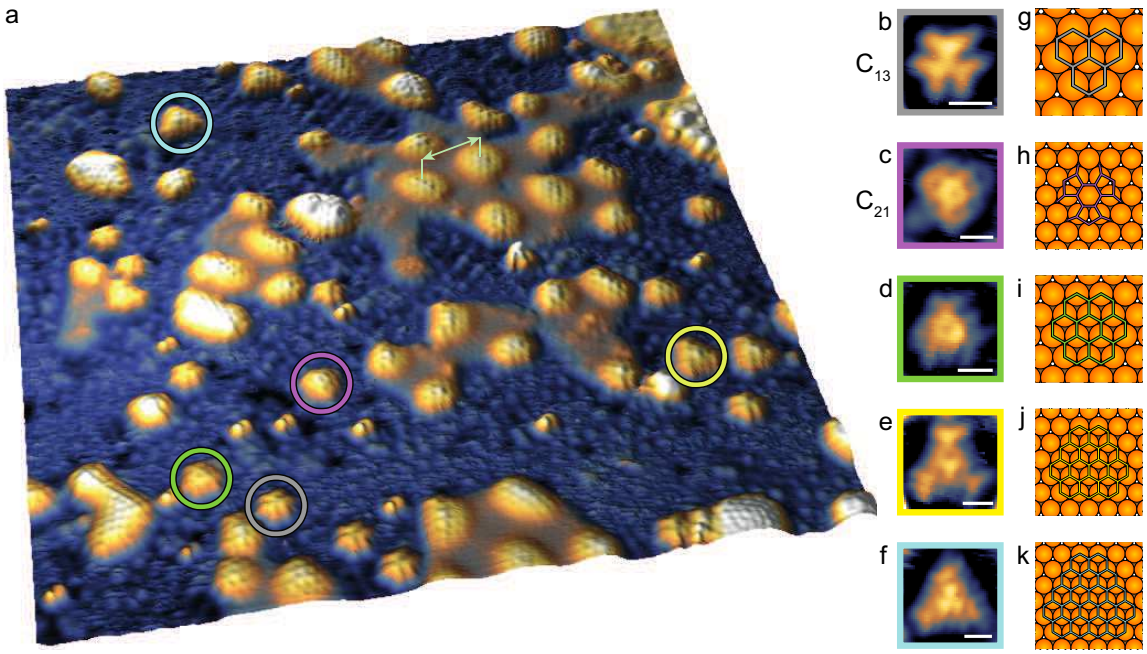

Figure 1: Size-selective C clusters generated by catalytic decomposition on a metal. (*a*) Three-dimensional STM topograph (bias voltage V_b=-2 V, tunneling current I_t=1 nA, 20×20 nm^2) of a Re(0001) surface after thermal decomposition. A family of polycyclic C clusters of well-defined size and crystalline orientation is observed. A double arrow highlights the 2.3 nm periodicity of the moiré patches. (*b*-*f*) are close-up views (scale bars = 0.5 nm), with a second-order polynomial background subtracted, of the five C clusters identified in (*a*), with the frames' colour matching that of the circles. (*g*-*k*) Ball-and-stick models of the five size-selective C clusters. The binding configuration observed in STM is represented, with one C atom on a *top* site of Re(0001) and the neighbor on the *fcc* site (g,i,j,k~~3C6, 7C6, 12C6 and 18C6 clusters~~), and the outer C atoms of the pentagons on *fcc* sites (h~~4C6-3C5 cluster~~).

The clean Re(0001) surface was exposed at room temperature to carbon-containing molecules, and further annealed under ultra-high vacuum (UHV) to trigger the catalytic decomposition reaction (see *Materials and Methods*) known to yield graphene.[10,13,30] We find that not only ethylene (here introduced in a controlled way under UHV), but also airborne carbon-containing species such as carbon monoxide (see specific discussion in *Materials and Methods*), can serve as precursor to the reaction and yield similar results. Thermal decomposition of the molecules under UHV is catalytically activated by the metal, and generates a high concentration of carbon adspecies at the surface. Beyond a threshold concentration

of these adspecies, graphene forms on the surface.[13]

A family of size-selective clusters

Annealing the sample (here to 800 K under UHV) yields graphene patches, with extension of the order of a few nanometers, as observed by STM (Figure 1~~*b*~~*a*). These patches exhibit a characteristic triangular pattern of about 2.3 nm in periodicity. Such a pattern is usually described with an analogy to a moiré effect, between the mismatched Re(0001) and graphene atomic lattices.[10,12,31] We find that small clusters coexist with these patches, five of which are highlighted in Figure 1. They all have three-fold symmetry, and all have a well-defined crystallographic orientation – which is actually mirrored from one terrace of the substrate to the neighbour terrace (See Figure S3). These features translate a symmetry breaking by the metallic surface. The occurrence of the clusters on the surface decreases as their size increases (Table S1). Close-up views of the clusters presented in Figures 1*b*-*f* reveal an atomic-scale contrast. As already mentioned, the STM images do not, nevertheless, directly unveil the atomic arrangement.

The way the clusters bind on the substrate has strong influence on their appearance in STM. The appearance reported here is much different from that of molecules having hydrogen-terminated edges,[17,20] and is characteristic of C-Re bonds at the edges of the clusters. Supporting this view, earlier thermal desorption experiments showed that already 100 K below the temperatures we used, all hydrogen atoms contained in ethylene (one of the precursors used here) have left the Re(0001) surface.[32]

Using geometry arguments, we now devise on the nature of the clusters and how they bind to Re(0001). The first constraints are the size of the objects as they appear in STM and their three-fold symmetry. We first focus on the smallest clusters (Figure 1*b*). They cannot comprise more than three benzene rings, and are hence dehydrogenated phenalene molecules (C_{13}~~3C6~~). In fact six possible configurations should be considered, each corresponding to a distinctive position of the two carbon sublattices with respect to the various possible binding

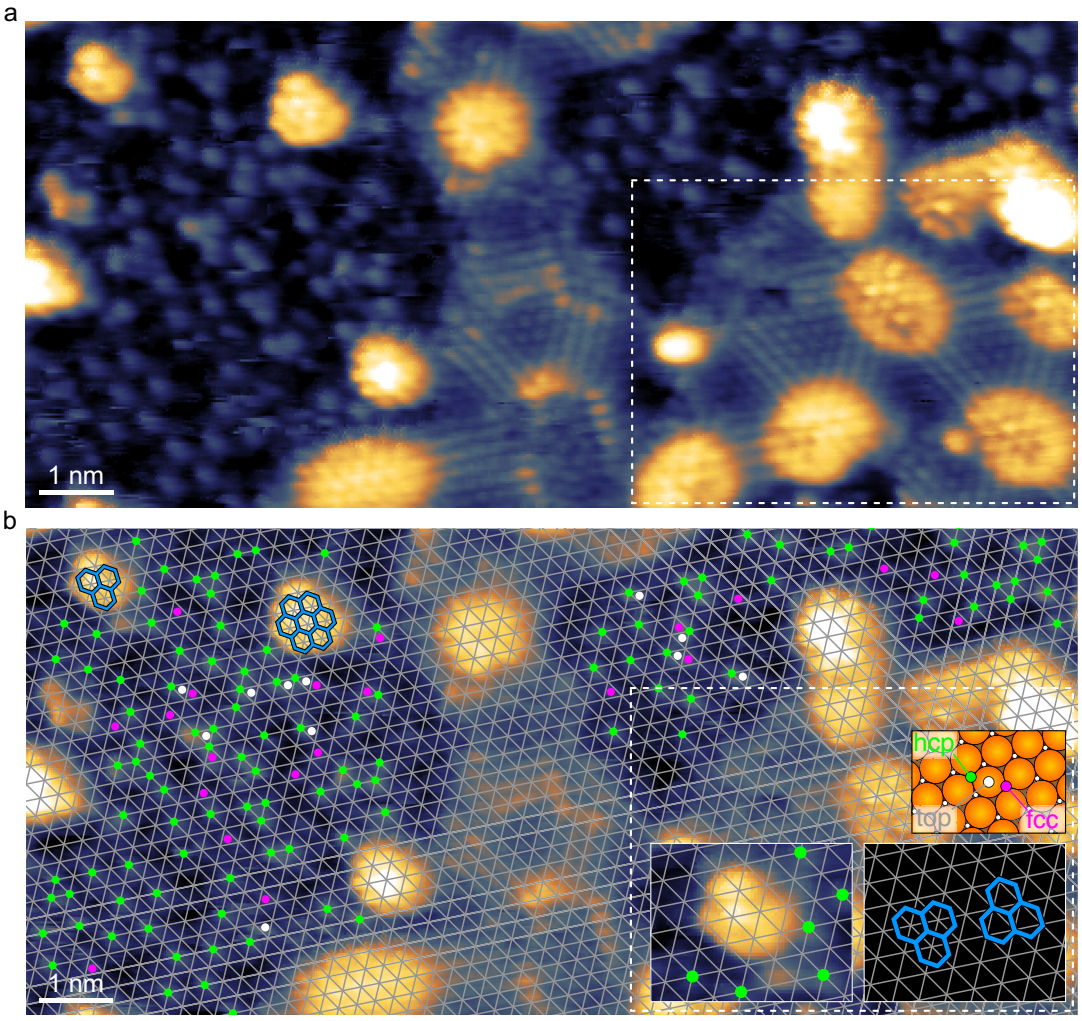

Figure 2: Coexisting C adatoms. (a) STM topograph (V_b=+0.5 V, I_t=5 nA) of a Re(0001) surface covered with C adatoms, size-selective C clusters, and graphene patches. (b) Same image as in (a), overlaid with a grid mapping the position of most of the C adatoms, and with a honeycomb-lattice marking the position of C atoms of the clusters. A majority of the C adatoms lie on the vertices of the grid (green dots), while others lie on upward-pointing triangles (~~orange~~pink dots) and even fewer on downward-pointing triangles (~~red~~white dots). Upper inset indicates these positions are respectively *hcp*, *fcc* and *top* sites (see text). Lower insets show a close-up view of the C_{13}~~3C6~~ cluster with two possible interpretations. A white dotted rectangle indicates the selected area~~a cut~~ analysed in greater detail in Figure 3.

sites on Re(0001) (Figure S4). By resolving the nature of all possible binding sites, we will now show that only one of these is compatible with our observations.

Chemical magnifying lenses

We address three specific crystallographic sites of the metal surface. They are especially important here since, as we will see, they are preferential binding sites of C atoms. They are so-called *top*, *hcp*, and *fcc* sites, corresponding respectively to the position of a surface Re atom, and to two hollow sites surrounded by three metal atoms. The latter two hollow sites differ only by the absence (*fcc*) and presence (*hcp*) of a metal atom underneath them (see inset in Figure 2*b*). They usually appear with very similar, often indiscernible contrast in STM, but we will now see how they can be discriminated.

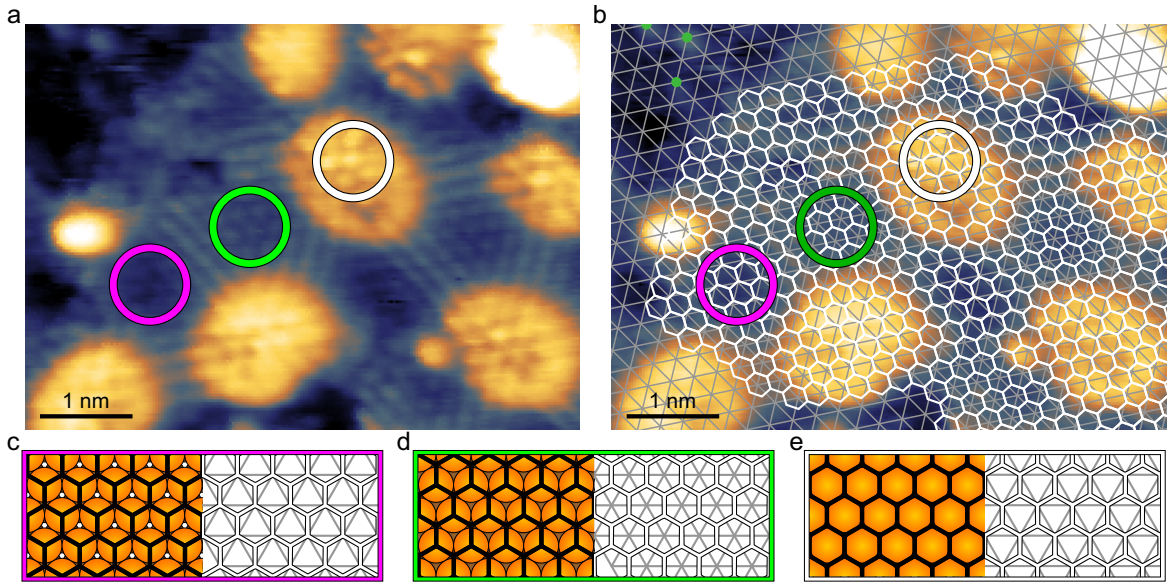

Figure 3: Chemical magnifying lenses, revealing the nature of the surface binding sites. (*a*) Selected area in the STM topograph shown in Figure 2~~Cut in the Figure 2 STM topograph~~ (V_b=+0.5 V, I_t=5 nA) focussing on the largest graphene patch. (*b*) Same image as in (*a*), overlaid with the same grid as in Figure 2, and with a honeycomb-lattice marking the position of C atoms of the graphene patch. ~~Red~~White, ~~orange~~pink, and green circles signal respectively the hill, *top-hcp* valley and *top-fcc* valley of the moiré superlattice. (*c-e*) Ball-and-stick models for the configuration of each moiré typical sites: *top-hcp* valley (*c*), *top-fcc* valley (*d*), and *fcc-hcp* hill (*e*).

To do so we turn our attention to the atomic-scale features that surround the graphene patches and clusters (Figure 2). They are bound to the substrate in a less random way than it may seem at first sight. Figure 2*a* shows that they locally form a (2×2) lattice with respect to the metal surface, also detected in our reflection high energy electron diffraction

experiments. In fact, it is possible to overlay the image with a regular grid, whose vertices are the most frequent position of the species (Figure 2*b*). There are exceptions, though, and we will shortly come back to them. The presence on the same image of a graphene patch with a moiré pattern makes it possible to ascribe the vertices of the grid to specific crystallographic sites on Re(0001) (*top*, *hcp*, or *fcc*). Indeed, the well-recognisable moiré sites can serve as a reference, and in this regard serve as the chemical equivalent of a magnifying lens.

We have previously shown that the moiré exhibits two low-lying regions that we refer to as valleys.[10] These two valleys have distinctive contrast in STM, revealed in Figure 3*a* and identified in Figure 3*b* with green and yellow circles. In one of the valleys, the two carbon sublattices that form graphene sit each on a *top* and a *fcc* site (green circle in Figure 3*b*, ball-and-stick model in Figure 3*d*). In this area, none of the C atoms sit on the vertices of the grid, which therefore corresponds to the *hcp* sites. Consistently, the vertices of the grid coincide with one in every two atoms in the other valley (*top*-*hcp*, Figure 3*c*) and in the hill (*fcc*-*hcp*, Figure 3*e*). Following the same line of thought, the *fcc* and *top* sites can be identified as the centres of respectively upward and downward-pointing triangles formed by the grid. This identification is further reinforced by the relative populations of C atoms on each site (see Figure S1 and associated discussion).

With this particularly valuable information in hand, usually missing to address the nature of small-sized C clusters observed by STM without ambiguity,[20] we will see that the qualitative appearance of the clusters in STM images allows to resolve their structure. Ultra-high resolution such as achieved with functionalized atomic force microscopy tips at low temperatures[33] is hence not indispensable here – standard STM instrumentation is sufficient.

The most straightforward implication of all the above considerations is that the clusters' edges align to the dense-packed metallic rows. Besides, getting back to the C_{13}~~3C6~~ cluster, it can be noticed on the lower insets of Figure 2*b* that two configurations are possible, and that for both the center of mass matches a *top* site. Among the six possible binding configurations of the C_{13}~~3C6~~ cluster (Figure S4), four are then readily discarded, again for

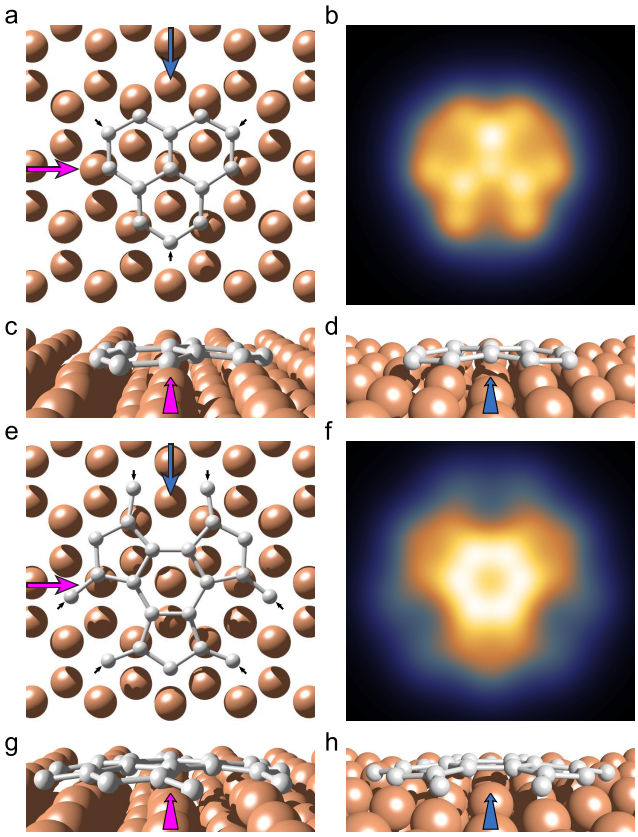

Figure 4: Resolved structure and binding configuration of size-selective C clusters. (*a*) Top-view ball-and-stick model of the C_{13}~~3C6~~ cluster on Re(0001) corresponding to the STM observations, with atomic positions optimised by the DFT calculations. (*b*) Simulated STM image of the corresponding configuration (V_b=-2 V, I_t=0.5-1 nA). (*c,d*) Side-views corresponding to (*a*), in two different directions indicated by the red (*c*) and blue (*d*) arrows corresponding to $\{10\bar{1}\}$ and $\{11\bar{2}\}$ directions respectively. (*e-h*) Same as (*a-d*), for the C_{21}~~4C6-3C5~~ cluster.

geometric reasons. In the two remaining configurations, one C sublattice sits on *top* sites while the other sits on either *fcc* or *hcp* sites (the two configurations will be referred to as *top-fcc* and *top-hcp* in the following).

Resolving the clusters' binding configuration and structure

To discriminate between both configurations we simulated STM images. We first optimised their geometry by DFT calculations taking van der Waals interactions into account (see *Materials and Methods*). We find that the clusters are dome-shaped, in agreement with

previous calculations[26] and that the bonds they form with Re atoms induce significant lattice distortion in the Re(0001) surface (Figures 4*a,c,d*). We then used the optimised geometry as an input for STM image simulation taking the scanning tip into account (see *Materials and Methods*).

A key-conclusion from these simulations is that for both *top-fcc* and *top-hcp* configurations, the strongest signal in STM is expected to match the position of the C atoms, to the exception of three atoms – those at the perimeter, with lowest coordination, sitting on *hcp* or *fcc* sites (Figures 4*a,b* and Figure S8~~7~~). This is true across a broad range of tip-sample bias voltages V_b, including at the 2 V value used in our experiments. This trait is a robust qualitative feature, which lifts the indetermination of the molecule's structure. Indeed, since we have already identified the *hcp* and *fcc* sites of the Re(0001) surface, our STM observations reveal C_{13}~~3C6~~ clusters with one C atom on a *top* site, and its neighbor on a *fcc* site. As a side note, the three C atoms at the periphery of the C_{13}~~3C6~~ cluster lie on *fcc* sites, and appear extinguished due to their strong bonding to the surface and to the cluster dome-shape. A similar conclusion can be drawn for the other clusters (Figures S5 and S6). We stress that very good agreement is obtained between the simulation (Figure 4*b*) and experimental data (Figure 1*b*). For completeness we also simulated STM images for the four other configurations, which clearly do not match with the experimental data (Figure S7).

This is to our knowledge the first clear-cut determination of the structure and binding configuration of size-selective C clusters prepared by thermal decomposition on metals. For (prohibitive) computational cost reasons, we do not address here the structure and binding configuration of the three largest clusters highlighted in Figures 1*d,e,f*, but simply propose a possible structure in Figures 1*i,j,k* (see *Supporting Information*).~~This was made possible by the discrimination of all binding sites of the substrate and of the STM signature of C atoms of distinctive chemical environment within the clusters. We now consider the three larger clusters highlighted in Figures 1*d,e,f*. Applying the same DFT methodology as above would be prohibitively consuming in terms of computing time, given the large size of the unit cell~~

~~(and large number of atoms) required to avoid spurious electronic interactions between the clusters in the periodic framework. Nevertheless, we believe that the above key-conclusion will still hold: the strong signal seen in STM matches with the position of the C atoms except for those at the periphery. Using the same reasoning as above, we find that the clusters are a 7C6 (Figure 1*d*) and two three-fold symmetric compact polygons with one kind of edge composed of two rings and the other one by three (12C6 for Figure 1*e*) or four (18C6 for Figure 1*f*) rings.~~

There are two species whose nature and binding to the substrate we have not discussed yet. One which appears slightly larger than C_{13}~~3C6~~ is the cluster shown in Figure 1*c*. Unlike the others it exhibits a central hexagonal ring, rotated by 30° with respect to the carbon lattice of the other clusters and of graphene. DFT calculations show that a 30°-rotated compact cluster consisting of seven hexagonal rings~~7C6~~ is not stable on the surface. We interpret this as a consequence of an unfavorable positioning of most of the C atoms with respect to *hcp*, *fcc*, and *top* sites, with at best some C atoms sitting on bridge sites (halfway between two neighbor Re atoms). The replacement of three of the peripheral hexagonal C rings by pentagons, corresponding to a dehydrogenated so-called sumanene molecule (C_{21}~~4C6-3C5~~), appears the most simple structure giving rise to more favorable atomic coincidences. To test this structure, we studied different possible configurations of clusters on Re(0001) with DFT calculations. Structure (meta)stability was only achieved when the three outer hexagons of the clusters opened to let six C atoms at the periphery sit on hollow sites, with two possible configurations, one for *hcp* sites, the other for *fcc* sites (see second row from the right on Figure 5*a* and Figure S10). Once more, STM image simulations reveal that strong signals in STM match with the position of the C atoms. As previously for C_{13}~~3C6~~, we hence establish that the observed configuration is that with the outer C atoms of the pentagons sitting on *fcc* sites. The geometry optimised by DFT is presented in Figures 4*e,g,h* and S10. It features significant distortions of both the carbon and rhenium structures. A very good agreement is found between the STM data and the

simulated image (compare Figure 4*f* and Figure 1*c*~~*d*~~).

The last species appears as a double-dot feature in Figure 1*a*~~*e*~~, but differently in other measurement runs. We ascribe this changing appearance to slight variations of the tip apex's morphology. This extreme sensitivity to the tip's details, a sign of a strong, very localised density of state, prevents us to get further insight into the nature of this species.

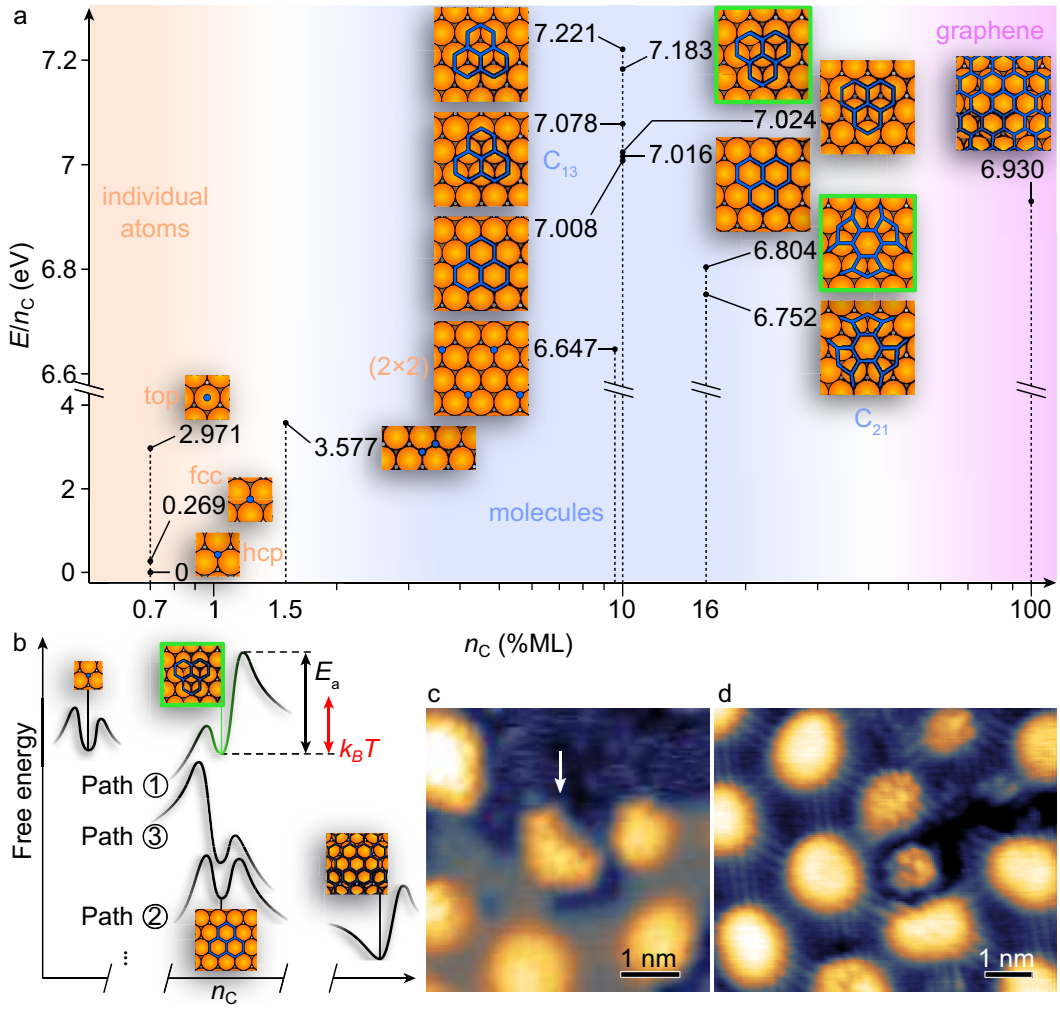

Figure 5: Thermodynamics and kinetics of the C clusters and graphene during the decomposition reaction. (*a*) Energy (E) divided by the number of C atoms (n_C) derived from the DFT calculations, for far-apart C atoms, two close-by C atoms, C clusters (C_{13}~~3C6~~ and C_{21}~~4C6-3C5~~) and infinite graphene. The green frames highlight the C_{13}~~3C6~~ and C_{21}~~4C6-3C5~~ observed in STM measurements. (*b*) Free-energy versus n_C diagram, where three possible evolution paths are schematized for C species on the surface (see text). (*c*) STM topograph (V_b=-2 V, I_t=1 nA) of a large~~18C6~~ cluster (of the same kind as in Figure 1*f*, marked with an arrow) incorporated by its edge to a graphene patch. (*d*) STM topograph (V_b=+0.03 V, I_t=6 nA) of a C_{13}~~3C6~~ cluster surrounded by graphene, at a more advanced stage of growth.

Kinetically-blocked metastable carbon clusters

So far we have largely eluded a discussion on the energetics of the C clusters. The configurations that we have determined above are minima in the potential energy landscape of the system, but in fact not global minima: they are metastable species. For instance, the C_{13}~~3C6~~ cluster observed in our STM measurements is in the fifth (out of six, see Table S2) least stable configuration and the C_{21}~~4C6-3C5~~ we observe is in the least stable binding configuration (of the two possible ones). This is summarized in Figure 5*a*, which shows the energy per C atom for the different binding configurations of C_{13}~~3C6~~ and C_{21}~~4C6-3C5~~, and compares them to the cases of individual C atoms and graphene. On a Rh(111) surface, Wang *et al.* already noticed that the STM observations were not compatible with a cluster in the lowest-energy configuration deduced by DFT.[20] They ascribed this disagreement to shortcomings in the DFT calculations, which were not for instance including van der Waals interactions. To further understand this disagreement, we have tested different implementations of the treatment of van der Waals interactions in our DFT calculations, and checked the effect of taking into account spin-polarisation effects. We confirm the robustness of the disagreement: the molecules that are observed in STM are indeed metastable, whatever the DFT simulation scheme employed.

Furthermore, not only do the observed C clusters adopt metastable configurations, but they are also significantly less stable than individual C adatoms sitting on *hcp* sites in a (2×2) lattice. For instance, the C_{13}~~3C6~~ cluster is 7.0 eV less stable (Figure 5*a*, note that energies are given per C atom in this figure), showing there is no thermodynamic driving force towards the formation of such C clusters. Even the C_{21}~~4C6-3C5~~ cluster proves 3.3 eV less stable than the (2×2) lattice. Under thermodynamical control, energy barriers to the formation of the clusters would be negligible compared to thermal energy, so species would obey a Boltzmann distribution according to their (meta)stability energies, and only a negligible number of metastable C clusters should be observed. This apparent paradox simply shows that the fate of the observed C clusters is instead under kinetic control, or that other effects

such as surface dissipation or entropy, play a role.[34]

To explicit this kinetic control, a few schematic paths leading from individual C atoms to stable and metastable clusters and graphene are proposed in Figure 5*b*. A first path (labelled '1' in Figure 5*b*) involves the metastable C_{13} or C_{21}~~3C6 or 4C6-3C5~~ clusters (or other metastable species) highlighted with green frames in Figure 5*a*. Along this first path, energy barriers for formation and transformation of the cluster are respectively low and high compared to thermal energy, so the formation of the cluster is facilitated while its evolution is blocked. These long-lived clusters formed at high temperature are still present once the sample has cooled down to room temperature for STM observations. Conversely, (meta)stable configurations of clusters not observed by STM correspond to other paths labelled '2' and '3' in Figure 5*b*. Path 2 is associated to lower activation energies for the evolution towards graphene. These short-lived species cannot be captured in our subsequent STM experiments. Finally path 3 involves high activation barriers for formation of species which will therefore in practice never form regardless of their stability.

Hints for distinctive energy barriers along each path can be inferred from DFT calculations. Irrespective of the detailed nature of the reaction path involving a particular cluster (this path may be complex given the number of degrees of freedom), we find that all configurations of the C_{13} clusters form strong bonds with the substrate *via* C atoms at their periphery. The nature of these bonds is different for the metastable (observed in STM) $top-fcc$(Figure S8p) and stable $hcp-fcc$ (Figure S8a) configurations. In the former case, sharing of electrons occurs between a C atom and a single Re atom, while in the latter case, sharing occurs within a hollow site, involving three Re atoms. The DFT calculations reveal a stronger charge density along the single nearest neighbor C-Re pair involved at the edge of the $top-fcc$ configuration, than along each of the three nearest neighbor C-Re pairs involved in the $hpc-fcc$ configuration (Figure S9). Even if altogether, these three pairs bring stronger stabilisation (the $hpc-fcc$ configuration indeed is the thermodynamically most stable one), individually they seem more tolerant (labile) towards a transformation of the

cluster to another species than the stronger single C-Re bond corresponding to the $top-fcc$ configuration.~~the observed 3C6 clusters (in a *top-fcc* configuration) form six strong C-Re bonds at the cluster edge. This is visualised on the iso-contour plot of the charge density displayed in Figure S10, and is consistent with the short C-Re bonds listed in Table S2. In contrast, the most stable 3C6 cluster (not observed in our experiments) with a *hcp-fcc* binding configuration forms no such strong bonds.~~

We stress that the formation of the most stable C_{13}~~3C6~~ cluster is not forbidden in our scenario. If it forms, its evolution must be easy, making it very short-lived at 800 K, and then in practice elusive. Extensive STM imaging of the samples' surface could indeed never detect the C_{13}~~3C6~~ cluster in this binding configuration. The metastable C_{13}~~3C6~~ cluster that we observe is on the contrary long-lived, and those we image are probably those that remained immobile during the preparation of the sample at 800 K. If they were not, they would presumably adopt the most stable binding configuration (which is more than 2 eV more stable).

While they have been interpreted as the mobile key-intermediate species towards graphene growth,[15,20] our analysis of the C clusters energetics rather proves they are kinetically blocked and immobile over extended durations including at temperatures characteristic of graphene growth. As a result, they are involved in reaction paths characterised by high activation energies, and their incorporation in graphene is strongly hindered.

The eventual fate of C clusters remains an intriguing question. Even though the individual evolution of C clusters cannot be monitored in our experiments, which take a snapshot of the surface after a given reaction time, in several instances the first steps of a cluster being incorporated are identified, as is the case of Figure 5*c* for a large cluster (of the same kind as that highlighted in Figures 1*f,k*, presumably a C_{51} cluster, see *Supporting Information*)~~18C6 cluster~~. This process is not easy, though: it involves a significant energy barrier. Indeed, even after increasing the temperature to 1100 K (compared to the 800 K temperature experiments discussed so far) and performing two annealing cycles in presence of ethylene, a

substantial density of metastable C_{13}~~3C6~~ clusters is observed, with a 50% reduction though. On the contrary, we observe no C_{21} cluster, consistent with earlier observations that partially cyclized clusters readily evolve towards other species upon temperature treatment.[34] This could be accounted for by energy barriers to the breaking of the carbon-metal bonds in the open cycles of the C_{21} clusters in the range of 1eV.[35] We note that for all kinds of clusters, entropic effects that would increase the rate of their transformation towards other species cannot be discarded.[34].

Figure 5*d* pictures a typical situation, where the graphene surface coverage is much higher, above 90%, and still these clusters are found with a typical density of one per 100 nm^2. ~~This density is twice less than in the previous experiments.~~ Strikingly, graphene surrounds the cluster, leaving Ångström-scale gaps without incorporating it. Incorporation actually seems to represent the limiting step in the growth of a full monolayer of graphene. In the future, developing growth strategies that avoid these kinetically hindered reaction paths may circumvent the formation of holes in graphene associated to the long-lived metastable clusters, and yield graphene of the highest quality. For this purpose we suggest the use of *ad hoc*-designed C precursors instead of the common short hydrocarbons.

Conclusions

We reported a uniquely large family of small size-selective C clusters ~~(3-18C6)~~ forming upon thermal decomposition of C-containing species on Re(0001). We provide the first clear-cut resolution of their structure, and on a more general note, of such kinds of clusters by use of standard high resolution STM. The methodology we introduced to do so is applicable to other kinds of molecules. It relies on small graphene patches and the moiré pattern that they exhibit, alternatively on dilute atomic lattices. While the latter lattice is formed together with the molecules and graphene in our case, for future works it seems straightforward to decorate the surface *a posteriori* with *ad hoc* atoms such as C or O atoms known to occupy

specific surface adsorption sites. These patterns disclose the tiny differences in the chemistry of distinct atomic-scale binding sites on the metal surface, which are often indiscernible with even high-resolution scanning probe microscopy.

With the help of DFT calculations and image simulations, we also provide an interpretation of the appearance of the C clusters in STM. The evolution of at least the smallest of these clusters appears strongly hindered kinetically. As such they coexist until advanced stages of graphene growth, and are for this reason obstacles to the achievement of high quality graphene. Increasing the growth temperature is a natural workaround to progressively suppress such metastable clusters that are otherwise very long-lived, and to achieve highest quality graphene by CVD – a long-standing objective in view of high performance applications. We stress that doing so is not possible in situations when graphene formation enters in competition with other processes that are thermally activated, such as the transformation of graphene into a metal carbide[11–13] or the dissolution of C inside the bulk metal.[11,13,14] We found that the former occurs on Re(0001) at hardly a few 10 K above the 1100 K temperature we have used to prepare graphene.

Finally, we note that the observation of size-selective C clusters is not restricted to the case of the Re(0001) surface, as they have also been reported on Ru(0001)[17] and Rh(111),[20] and that although so far unresolved, clusters with related appearance in STM have been observed as well on Pt(111)[23] or Ir(111)[25] surfaces.

Materials and Methods

A Re(0001) single crystal, bought from Surface Preparation Laboratory, was prepared inside the same UHV system (10^{-10} mbar base pressure) where the STM measurements were performed, by repeated cycles of Ar ion bombardment with 2 keV energy at 1020 K and subsequent fast annealing to 1570 K. Thin Re(0001) (50 nm-thick) films were also used as substrate, yielding equivalent results. They were deposited on α-Al_2O_3(0001) by atomic beam epitaxy[10] in a separate UHV system, and introduced (after exposure to atmospheric

pressure) in the UHV system where STM measurements were done.

The Re(0001) surface exposed to atmospheric pressure was first annealed to 570 K for 5 h under UHV, and then merely annealed at 800 K, yielding graphene patches and C clusters. The C precursor is in this case presumably an airborne species with a substantial sticking coefficient on Re(0001) and decomposing on it upon thermal treatment. CO (fractions of ppm in air, and decomposed on Re(0001) at a few 100 K[36]) is the most obvious candidate. The same products (graphene and C clusters) are obtained by annealing a clean Re(0001) surface, freshly prepared under UHV and covered with a controlled amount of ethylene (C_2H_4) deposited at 300 K. A high graphene surface coverage was obtained by exposing Re(0001) to 10^{-8} mbar of C_2H_4 at 300 K and annealed twice between 300 and 1100 K. In this case also we observe C clusters and graphene on the surface.

STM measurements were performed at room temperature using a Omicron-STM1 set-up coupled under UHV to the chamber where the samples were prepared. Chemically-etched W tips were employed for STM imaging.

DFT calculations were performed using the `VASP` code, with the projector augmented wave (PAW) approach.[37,38] The exchange correlation interaction is treated within the general gradient approximation parametrized by Perdew, Burke and Ernzerhof (PBE).[39] Van der Waals interactions have been accounted for using Grimme corrections.[40] More details are given in the Supplementary Information. The energy per C atom (Figure 5*a*) is computed by removing the energy of a bare Re surface E_{surf}, and using a single C atom on a *hcp* site as a zero-energy reference $E_{\mathrm{ref}} = E_{1\mathrm{C},hcp} - E_{\mathrm{surf}}$. For a configuration of total energy E_{tot} containing n_{C} carbon atoms, the energy per carbon atom E is hence $E = (E_{\mathrm{tot}} - E_{\mathrm{surf}})/n_{\mathrm{C}} - E_{\mathrm{ref}}$.

DFT calculations within a local-orbital formulation were performed using the `FIREBALL` code,[41–43] with the exchange-correlation (XC) effects accounted for by a local density approximation (LDA) functional,[41] and the ion-electron interaction modelled by means of norm-conserving scalar-relativistic pseudopotentials.[44] More details are given in the Supplementary Information. The constant-current ($I_t \sim$ 0.5-1 nA) STM images have been computed

at V_b=-2.5 to 0 V, by using a Keldysh-Green function formalism, with the first-principles tight-binding Hamiltonian obtained from FIREBALL.[42,45–47] The electronic properties of both the tip and the sample were taken into account. The sample corresponds to one of the DFT-calculated configurations. The tungsten tip was simulated by five protruding atoms (one at the apex) attached to an extended W(100) crystal.

Acknowledgement

The authors thank Dr. Frédéric Chérioux for fruitful discussions. J.I.M and J.A.M.-G. acknowledge financial support by the Spanish MINECO (Grants MAT2014-54231-C4-1-P and RYC-2015-17730) and the EU via the innovation program under grant agreement No. 696656 (Graphene Core1-Graphene-based disruptive technologies). VASP calculations were performed using HPC resources from GENCI-IDRIS (Grant 2017-A0020907655).

Supporting Information Available

Supporting information comprises details about materials and methods, supplementary STM images of the C clusters and of an intentionally deposited oxygen phase, a description (ball-and-stick models, electronic density maps, energies, STM simulations) of each possible binding configuration of the 3C6 cluster, and a statistical survey of species found on the surface.

This material is available free of charge via the Internet at http://pubs.acs.org/.

References

(1) Castro Neto, A. H.; Guinea, F.; Peres, N. M. R.; Novoselov, K. S.; Geim, A. K. Rev. Mod. Phys. **2009**, 81, 109–162.

(2) Ferrari, A. C. et al. Nanoscale **2015**, 7, 4598–4810.

(3) Tetlow, H.; Posthuma de Boer, J.; Ford, I.; Vvedensky, D.; Coraux, J.; Kantorovich, L. Phys. Rep. **2014**, 542, 195–295.

(4) Dedkov, Y.; Voloshina, E. J. Phys. Condens. Matter **2015**, 27, 303002.

(5) Pollard, A. et al. Angew. Chem. Int. Ed. 49, 1794–1799.

(6) Sicot, M.; Bouvron, S.; Zander, O.; Rüdiger, U.; Dedkov, Y. S.; Fonin, M. Appl. Phys. Lett. **2010**, 96, 093115.

(7) Sutter, E.; Albrecht, P.; Wang, B.; Bocquet, M.-L.; Wu, L.; Zhu, Y.; Sutter, P. Surf. Sci. **2011**, 605, 1676 – 1684.

(8) Zhang, H. G.; Sun, J. T.; Low, T.; Zhang, L. Z.; Pan, Y.; Liu, Q.; Mao, J. H.; Zhou, H. T.; Guo, H. M.; Du, S. X.; Guinea, F.; Gao, H.-J. Phys. Rev. B **2011**, 84, 245436.

(9) Estyunin, D. A.; Klimovskikh, I. I.; Voroshnin, V. Y.; Sostina, D. M.; Petaccia, L.; Di Santo, G.; Shikin, A. M. JETP **2017**, 125, 762–767.

(10) Tonnoir, C.; Kimouche, A.; Coraux, J.; Magaud, L.; Delsol, B.; Gilles, B.; Chapelier, C. Phys. Rev. Lett. **2013**, 111, 246805.

(11) Dong, G. C.; van Baarle, D. W.; Rost, M. J.; Frenken, J. W. M. New J. Phys. **2012**, 14, 053033.

(12) Qi, Y.; Meng, C.; Xu, X.; Deng, B.; Han, N.; Liu, M.; Hong, M.; Ning, Y.; Liu, K.; Zhao, J.; Fu, Q.; Li, Y.; Zhang, Y.; Liu, Z. J. Am. Chem. Soc. **2017**, 139, 17574–17581.

(13) Miniussi, E.; Pozzo, M.; Menteş, T.; Niño, M.; Locatelli, A.; Vesselli, E.; Comelli, G.; Lizzit, S.; Alfè, D.; Baraldi, A. Carbon **2014**, 73, 389–402.

(14) McCarty, K. F.; Feibelman, P. J.; Loginova, E.; Bartelt, N. C. Carbon **2009**, 47, 1806–1813.

(15) Wang, B.; König, M.; Bromley, C. J.; Yoon, B.; Treanor, M.-J.; Garrido Torres, J. A.; Caffio, M.; Grillo, F.; Früchtl, H.; Richardson, N. V.; Esch, F.; Heiz, U.; Landman, U.; Schaub, R. J. Phys. Chem. C **2017**, 121, 9413–9423.

(16) Zhang, H.; Fu, Q.; Cui, Y.; Tan, D.; Bao, X. J. Phys. Chem. C **2009**, 113, 8296–8301.

(17) Cui, Y.; Fu, Q.; Zhang, H.; Bao, X. Chem. Commun. **2011**, 47, 1470–1472.

(18) Donner, K.; Jakob, P. J. Chem. Phys. **2009**, 131, 164701.

(19) Lu, J.; Yeo, P. S. E.; Gan, C. K.; Wu, P.; Loh, K. P. Nat. Nanotech. **2011**, 6, 247–252.

(20) Wang, B.; Ma, X.; Caffio, M.; Schaub, R.; Li, W.-X. Nano Lett. **2011**, 11, 424–430.

(21) Loginova, E.; Bartelt, N. C.; Feibelman, P. J.; McCarty, K. F. New J. Phys. **2009**, 11, 063046.

(22) Jiang, H.; Wu, P.; Hou, Z.; Li, Z.; Yang, J. Phys. Rev. B **2013**, 88, 054304.

(23) Land, T. A.; Michely, T.; Behm, R. J.; Hemminger, J. C.; Comsa, G. Appl. Phys. A **1991**, 53, 414–417.

(24) Johánek, V.; De La Ree, A. B.; Hemminger, J. C. J. Phys. Chem. C **2009**, 113, 4441–4444.

(25) Coraux, J.; N'Diaye, A. T.; Engler, M.; Busse, C.; Wall, D.; Buckanie, N.; Heringdorf, F.-J. M. z.; Gastel, R. v.; Poelsema, B.; Michely, T. New J. Phys. **2009**, 11, 023006.

(26) Lacovig, P.; Pozzo, M.; Alfè, D.; Vilmercati, P.; Baraldi, A.; Lizzit, S. Phys. Rev. Lett. **2009**, 103, 166101.

(27) Yuan, Q.; Gao, J.; Shu, H.; Zhao, J.; Chen, X.; Ding, F. J. Am. Chem. Soc. **2012**, 134, 2970–2975.

(28) Gao, J.; Ding, F. Angew. Chem. Int. Ed. **2014**, 126, 14255–14259.

(29) Gao, J.; Ding, F. J. Clust. Sci. **2015**, 26, 347–360.

(30) Miniussi, E.; Pozzo, M.; Baraldi, A.; Vesselli, E.; Zhan, R. R.; Comelli, G.; Menteş, T. O.; Niño, M. A.; Locatelli, A.; Lizzit, S.; Alfè, D. Phys. Rev. Lett. **2011**, 106, 216101.

(31) Artaud, A.; Magaud, L.; Le Quang, T.; Guisset, V.; David, P.; Chapelier, C.; Coraux, J. Sci. Rep. **2016**, 6, 25670.

(32) Ducros, R.; Housley, M.; Alnot, M.; Cassuto, A. Surf. Sci. **1978**, 71, 433–446.

(33) Gross, L.; Mohn, F.; Moll, N.; Liljeroth, P.; Meyer, G. Science **2009**, 325, 1110–1114.

(34) Riss, A.; Paz, A. P.; Wickenburg, S.; Tsai, H.-Z.; De Oteyza, D. G.; Bradley, A. J.; Ugeda, M. M.; Gorman, P.; Jung, H. S.; Crommie, M. F.; Rubio, A.; Fischer, F. R. Nat. Chem. **2016**, 8, 678–683.

(35) Vang, R. T.; Honkala, K.; Dahl, S.; Vestergaard, E. K.; Schnadt, J.; Lægsgaard, E.; Clausen, B. S.; Nørskov, J. K.; Besenbacher, F. Nat. Mater. **2005**, 4, 160.

(36) Ducros, R.; Alnot, M.; Ehrardt, J. J.; Housley, M.; Piquard, G.; Cassuto, A. Surf. Sci. **1980**, 94, 154–168.

(37) Kresse, G.; Hafner, J. Phys. Rev. B **1993**, 47, 558–561.

(38) Kresse, G.; Joubert, D. Phys. Rev. B **1999**, 59, 1758.

(39) Perdrew, J. P.; Burke, K.; Ernzerhof, M. Phys. Rev. Lett. **1996**, 77, 3865–3868.

(40) Grimme, S. J. Comput. Chem. **2006**, 27, 1787–1799.

(41) Jelínek, P.; Wang, H.; Lewis, J. P.; Sankey, O. F.; Ortega, J. Phys. Rev. B **2005**, 71, 235101.

(42) Lewis, J. P.; Jelínek, P.; Ortega, J.; Demkov, A. A.; Trabada, D. G.; Haycock, B.; Wang, H.; Adams, G.; Tomfohr, J. K.; Abad, E.; Wang, H.; Drabold, D. A. Phys. Status Solidi B **2011**, 248, 1989–2007.

(43) Demkov, A. A.; Ortega, J.; Sankey, O. F.; Grumbach, M. P. Phys. Rev. B **1995**, 52, 1618–1630.

(44) Fuchs, M.; Scheffler, M. Comput. Phys. Commun. **1999**, 119, 67–98.

(45) Blanco, J. M.; González, C.; Jelínek, P.; Ortega, J.; Flores, F.; Pérez, R. Phys. Rev. B **2004**, 70, 085405.

(46) Blanco, J. M.; Flores, F.; Pérez, R. Prog. Surf. Sci. **2006**, 81, 403–443.

(47) González, C.; Snijders, P. C.; Ortega, J.; Pérez, R.; Flores, F.; Rogge, S.; Weitering, H. H. Phys. Rev. Lett. **2004**, 93, 126106.

Graphical TOC Entry